Analyst

Accepted Manuscript

This article can be cited before page numbers have been issued, to do this please use: J. Yao, Z. Zhang, Z. Deng, Y. Wang and Y. Guo, *Analyst*, 2017, DOI: 10.1039/C7AN01224A.

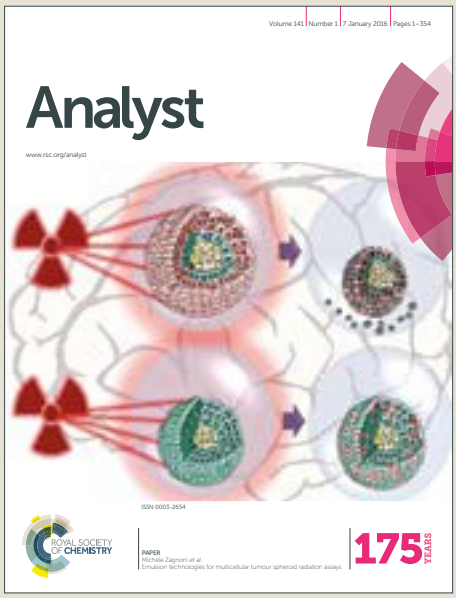

ROYAL SOCIETY OF CHEMISTRY

rsc.li/analyst

View Article Online
DOI: 10.1039/C7AN01224A

Analyst

ARTICLE

An enzyme free electrochemical biosensor for sensitive detection of miRNA with high discrimination factor by coupling strand displacement reaction and catalytic hairpin assembly recycling

Received 00th January 20xx,
Accepted 00th January 20xx

DOI: 10.1039/x0xx00000x

www.rsc.org/

Juan Yao,[a] Zhang Zhang,[b] Zhenghua Deng,[b] Youqiang Wang[a] and Yongcan Guo[a]*

An isothermal, enzyme free, ultra-specific and ultra-sensitive protocol for electrochemical detection of miRNAs is proposed based on toehold-mediated strand displacement reaction (SDR) and non-enzymatic catalytic hairpin reaction (CHA) recycling. SDR was first triggered only in the presence of target miRNA and this process also sinking other miRNA interferences similar in target sequence, thus guaranteed high discrimination factor and could be used in rare content miRNA detection with amounts interferences similar in target sequence. The output protector strand then triggered enzyme free CHA amplification and generates plenty hairpin self-assembly product. This process in turn influences SDR equilibrium moves to the right and generates amounts protector output to ensure analysis sensitivity. Compared with traditional CHA, our proposed method greatly improved signal to noise ratio and shows excellent performance in rare miRNA detection with miRNA analogues interference. Under the optimal experimental conditions and using square wave voltammetry, the established biosensor could detect target miRNA-21 down to 30 fM (S/N=3) with a dynamic range from 100 fM to 2 nM, and discriminate rare target miRNA-21 from mismatched miRNA with high selectivity. This method holds great promise in miRNA detection from human cancer cell lines and would be a versatile and powerful tool for clinical molecular diagnostics.

Introduction

MicroRNAs (miRNAs) are small class of endogenous, non-coding RNA molecules ranging from 17 to 22 nt in size, similar in sequence among family members and suppress protein translation through posttranscriptional mechanisms by matching predominately to the 3'-untranslated region (3'-UTR) of the target gene[1-3]. Since the discovery of miRNAs in circulation, large amounts of miRNA-related biological studies have confirmed that the dysregulated expression of miRNAs contributes to tumor metastasis, stem-cell differentiation and renewal, and viral replication[4-6]. These characteristics make miRNAs a new group of promising biomarkers for early clinical diagnosis, and their sensitive and selective qualification possesses great significance in the clinical applications of tumor molecular diagnosis[7, 8].

Currently available quantitative miRNAs detection methods have always been a tough call owing to their short and extremely homologous sequences and low concentrations thus influence detection selectivity and sensitivity. Conventional analytical methods, including northern blotting[9], microarray-based techniques[10] and real-Time quantitative reverse transcription PCR (qRT-PCR)[11] are widely utilized for miRNA analysis. Though these methods have showed some merits, they still suffer from some drawbacks in practical applications such as semi-quantitative, laborious, and requiring expensive equipment. Hence, biosensing strategies, including electrochemical[12-14], luminescence[15-17] and colorimetric biosensors[18, 19], have become a class of powerful tools for accurate and quantitative miRNA expression. Among these methods, electrochemical biosensors have recently gained special attention due to their high sensitivity and selectivity, simple instrumentation, low production cost, and the fact that they are fast, accurate, compact, portable, and inexpensive.

The key points evaluate the performance of a biosensor are: sensitivity, where analytical limits of detection and quantification are low enough to reliably measure miRNAs at biologically relevant levels; selectivity, where biosensor could discriminate target miRNA from interfering miRNAs (especially one nucleotide differences). In order to further improve the detection sensitivity of miRNAs, various amplification strategies have been developed, such as catalytic hairpin self-assembly (CHA)[20, 21], rolling circle amplification (RCA)[22, 23], hybridization chain reaction (HCR)[24,

[a] Department of Laboratory Medicine, Affiliated Traditional Chinese Medicine Hospital of Southwest Medical University, Luzhou, 646000, P. R. China. swtcmlab@163.com and 396497795@qq.com; Tel: +86 830 3165223
[b] Department of Laboratory Medicine, Affiliated Hospital of Southwest Medical University, Luzhou, 646000, P. R. China.
Electronic Supplementary Information (ESI) available: [Fig. S1-S6 and Table S1-S4].
See DOI: 10.1039/x0xx00000x

View Article Online
DOI: 10.1039/C7AN01224A

25], enzymatic signal amplification[26, 27], and nanomaterial-based assay[28, 29]. Due to the hybridization between miRNA target and probe does not strictly obey Watson-Crick base pairing rules, interfering miRNAs may hybridized to probe resulted in false-positive result. In order to further improve the detection selectivity of miRNAs, various techniques to improve the selectivity of nucleic acids hybridization were developed including strand displacement reaction[30-32], molecular beacons[33], triple-stem clamp nanoswitches[34] and enhance the hybridization reaction temperature near melting temperature[35]. Although current research is ongoing to amplify signal and restrain background, lots of existing DNA-amplification protocols have not yet found a very reasonable way to integrate the two aspects into one system, which suffered from elevated background or poor amplification efficiency.

SDR (contains three steps: toehold domains initiate binding, branch migration and strand displacement completes) utilizes the thermodynamic properties enable near-optimal single nucleotide discrimination of double-strand probe and perform robustly across diverse temperature, salt and concentration conditions. CHA as an enzyme free amplification method, rely only on hybridization and toehold mediated strand-exchange reactions in order to achieve amplification, has been proven to be powerful in amplifying and transducing signals at the terminus of nucleic acid amplification reactions. Although got over hundreds of difficulties, enzymatic amplification, CHA shows great background signal drawback caused by the nonspecific CHA products in the absence of target, which may counteract the selectivity of CHA-based signal amplification methodologies and compromise their analytical performance. In this article, aiming to overcome the above-mentioned technique bottleneck and achieve an appropriate trade-off between acceptable sensitivity and selectivity, we coupled toehold-mediated SDR and CHA to achieve the optimum balance between sensitivity and selectivity. A simple, universal, sensitive and specific electrochemical miRNA biosensor was developed based on SDR and CHA for the first time. SDA guarantees lower background thus ensure high selectivity and the excellent amplication effects of CHA ensured high sensitivity. The designed platform exhibited excellent analytical performance towards miRNA determination and might become a potential alternative tool for detection of miRNA in biomedical research and early clinical diagnosis.

Experimental

Reagents and apparatus

DNA oligonucleotides were synthesized and HPLC purified by Sangon Inc., miRNA-21 was obtained from Takara (Dalian, China) and their sequences are listed in Table S1, domains are listed in Table S2. All oligonucleotides were dissolved in tris-ethylenediaminetetraacetic acid (TE) buffer (pH 8.0, 10 mM Tris–HCl, 1 mM EDTA) and stored at -20 °C, which were diluted in hybridization buffer (20 mM Tris-HCl contains 100 mM NaCl, pH 7.5) prior to use. MCF-7 cell lines (early stage breast cancer cell) was purchased from American Type Culture Collection (ATCC, Manassas, VA, USA) and maintained in Dulbecco's modified Eagle's medium (DMEM, Hyclone, USA) supplemented with 10% fetal bovine serum (FBS, Gibco, USA) and 100U·mL^{-1} streptomycin/penicillin at 37 °C in 5% of CO_2. 6-Mercapto-1-hexanol (MCH), Hexaammineruthenium (III) chloride ($[Ru\text{-}(NH_3)_6]^{3+}$, RuHex) and Diethylpyrocarbonate (DEPC) were purchased from Sigma-Aldrich (St. Louis, MO, USA). All solutions were prepared with ultrapure water obtained from a Milli-Q water purification system (Millipore, USA) with resistivity of 18.2 MΩ·cm^2. Electrochemical measurements including square wave voltammetry (SWV, within the potential range from 0-0.4 for characterization and −0.45 to 0.15 V for methylene blue signal detection under pulse amplitude of 25 mV and afrequency of 25 Hz), electrochemical impedance spectroscopy (EIS, under open circuit potential and bias potential is set to 0) and chronocoulometry measurements (See in Text S1) were carried out on a CHI660D electrochemical workstation (Shanghai Chenhua Instruments Co. Ltd., China) with a conventional three electrode system composed of platinum wire as auxiliary, Ag/AgCl electrode as reference and a 3-mm diameter gold electrode as working electrode. All spectro-fluorometric measurements were performed at 25 °C with an Enspire multimode microplate reader (Perkinelmer, USA).

DNA Sequences and Design

DNA sequences and modifications are based on a DNA strand displacement and catalytic hairpin assembly reported by Zhang et al.[31] and Li et al. [36] and modified by hand to generate allosteric toehold sequences. All DNA sequences were then analyzed using Mfold to ensure minimal crosstalk between unrelated domains. All DNA oligonucleotides were denatured at 95 °C for 5 min and cooled down 5 °C per minute to the room temperature.

Preparation of electrochemical biosensor

The bare gold electrode was polished with 50 nm alumina slurries and ultrasonically treated in ultrapure water for a few minutes, followed by soaking in piranha solution (H_2SO_4:H_2O_2=3:1) for 10 min to eliminate other substances. Finally, electrochemical cleaning was conducted at the electrode with 30 successive CV scans from 0.2 to 1.6 V in 0.5 M H_2SO_4, further rinsed in distilled water and dried with nitrogen. The pretreated gold electrode was rinsed with ultrapure water and allowed to dry at room temperature. 10 μL of 1 μM thiolated capture probe was dropped on the pretreated gold electrode surface (incubated overnight at 4 °C) and anchored via Au-S bond between the gold electrode and the 5'-hexanethioltethers (C_6SH), whose length matches that of MCH. After washed with hybridization buffer, the electrode was immersed into 10 μL of 1 mM MCH for 1 h to obtain well-aligned DNA monolayer which would occupy the left bare sites. The electrode was further rinsed with the washing buffer to obtain the electrochemical DNA biosensor. Equal 30 μL equimolar (3 μM) protector/complement was first incubated with H1 and H2 in hybridization buffer at room temperature to obtain reaction conjugation. Various concentrations of target were added into the

View Article Online
DOI: 10.1039/C7AN01224A

resulting solution, subsequently, 10 μL various concentrations of miRNA 21 were added into the resulting solution for reasonable time. Then, 10 μL obtained mixture solution was dropped onto the modified gold electrode for electrochemical test.

Results and discussions

Working principle of the proposed method

The principle of fabricated electrochemical DNA biosensor is depicted in Scheme 1. Target miRNA was first reacted with double-strand probe and generates protector output via toehold mediated SDR (see in Scheme 1A). This process ensures high discrimination factor (DF, defined as the ratio of the signal increase observed with the target and the mismatched target) contributed to toehold-mediated strand displacement systems used competing sequences with perfect complementarily to the matched targets and generates protector input thus avoiding the interference spurious targets from solution. As shown in Scheme 1B, the output protector can hybridize with methylene blue (as electrochemical indicator) tagged hairpin H1 and unfold the hairpin structure of H1. The opened H1 assembles with H2 to displace the protector. Next, the liberated protector strands hybridize with the hairpin sequence of H1 again and initiate the CHA cycles, resulting in the generation of massive H1–H2 complexes. Afterwards, the H1–H2 complexes can specifically hybridize with the capture probes immobilized on the sensor surface (see in Scheme 1C).

<Scheme 1>

Feasibility of the proposed strategy

The selectivity of strand displacement reaction may be attributed to the formation of spurious bubbles (induced by mismatch, deletion or insertion), which may decrease the reaction rate or hinder the branch migration of this reaction. Kinetic analysis of target and spurious single base mismatch target were performed to investigate the discrimination ability of SDR, CHA and our proposed strategy. As shown in Fig. 1A, the fluorescence increased when added target sequence, whereas mismatch target added to this system, minimal changes in fluorescence intensity was observed compared with that in the complementary target (DF equals to 13.6). The result in Fig. 1B shows that CHA shows the poor discriminate ability between target and single base mismatch, this may due to the unspecified assembly of hairpins (DF equals to 5.3). The result in Fig. 1C shows that when SDR and CHA were combined, the signal with target and single base variant targets are clearly differentiated. The improved DF equals to (37.3) of this proposed coupling strategy may due to the sustained cascade recognition events.

< Fig. 1>

Characterization of electrode surface modification

EIS and SWV measurements were adopted in 0.1 M KCl (pH 7.0) containing 5 mM $[Fe(CN)_6]^{3-/4-}$ to characterize the established electrochemical biosensor. The semicircle diameters at high frequency region reflect the electron transfer resistance (Ret) which controls the electron transfer kinetics at the electrode interface. As shown in Fig. 1A, bare electrode exhibited an almost straight line (curve a) reflecting the outstanding electrochemical conductivity. When the thiolated capture DNA was self-assembled onto the bare electrode via Au-thiol binding, the Ret increased (curve b). This was because that the negatively charged phosphate backbone of the oligonucleotides produced an electrostatic repulsion force to $[Fe(CN)_6]^{3-/4-}$. However, after MCH was immobilized on the electrode surface, the Ret increased (curve c) attributed to that the bio-macromolecules could obstruct the electron transfer. Afterwards, the remaining capture DNA hybridized with the H1-H2 complexes without the participation of target miRNA, the Ret slightly increased (curve d). With participation of target miRNA, the Ret increased significantly (curve e), which indicated that only a few of H1 and H2 can initiate reaction in the absence of the target, and in the presence of target miRNA catalysis, a large amount of H1-H2 complexes were obtained. The EIS data were fitted according to a Randles equivalent electrical circuit (inset, Fig. 2A). The equivalent electrical circuit consisted of an active electrolyte resistance (Rs) in a series with a constant phase element (CPE, 6.03E+05) and an electro-transfer resistance (Ret) in parallel with Warburg impedance (Z_W). These results were in a good agreement with those obtained from SWV measurements (Fig. 2B), in which the peak currents varied upon the assembly and binding processes. Both results of EIS and SWV proved that the biosensor worked indeed as described in the principle scheme. Further, electrode active surface area was calculated to be 0.028 cm^2 via cyclic voltammetry and probe density was estimated to be $7.53\times10^{12}/cm^2$ via chronocoulometry (details see Fig. S1 and S2).

< Fig. 2>

Optimization of experiment conditions

In order to achieve the best analytical performance, different crucial experiment parameters including toehold length, incubating temperature, incubation time and hairpin H1, H2 concentrations were investigated (with 1 nM target or mismatch target). When a reaction condition was optimized, the other conditions were kept in the optimized condition or the longest reaction times and the highest concentrations.

"Toehold exchange" as a novel type of strand displacement reaction, have been supposed to possess good discrimination ability and subsequently used in many strategies to achieve specialize detection. To evolution DF of toehold exchange mediated strand displacement reaction, the dsProbe is a preformed partial duplex that consists of a FAM-labelled protector strand and a Dabcyl-labeled complement strand (See in Fig. S3). After incubation with the desired target, the protector strand is competitively displaced from the original duplex, and fluorescence is tuned to release. In

View Article Online
DOI: 10.1039/C7AN01224A

this article, initial toehold was set as 7 for the reason toeholds length are typically from 4 to 10 nt. The main factor influence sensitivity and selectivity is the length of separation toehold due to its influence on the kinetic and thermodynamic of displacement reaction. To obtain the optimal performance of this strategy, we used four different protector probes containing different lengths of separation toehold (7/6, 7/4 probes and 7/2 toehold exchange probe, see in Fig. 3). The DF represents the ability of the proposed probe to distinguish point mutation in a target sequence. The signals enhanced with the decrement of separation toeholds. Considering DF, 7/4 probe was used as optimal choice.

< Fig. 3>

Relative high concentration of hairpins can increase the self-assembly of hairpins, leads to deteriorative noise thus influence sensitivity (secondary structure of H1 and H2 are shown in Fig. S4 using Mfold software). To avoid the non-specific signal induced by non-specific background amplification, the effect of hairpin H1 and H2 concentrations were investigated. The maximum value of DF was achieved at the H1 concentration of 100 nM and H2 concentration of 75 nM, thus 100 nM H1 and 75 nM H2 was chosen as the optimal conditions (See in Fig. 4A and Fig. 4B). Incubation time is another important parameter for SDA and CHA reaction. To optimize the incubation time, different incubation time was analyzed ranging from 0 min to 40 min. As shown in Fig. 4C, the signal to noise ratio ascended with the increase of incubation time. When the incubation time extended to 20 min, the signal to noise ratio showed deteriorated. Therefore, 20 min was chosen as the optimal incubation time. Temperature, which determines the molecule collisions probabilities, is an important parameter of reaction kinetics. In CHA, incubation temperature is a key factor that influences the stability and interaction of the hairpin probes. With lower incubation temperature, hairpin probes could not get a sufficient collision probability with target, thus greatly reducing the formation of amplification products. On the contrary, with higher incubation temperature, the selectivity of CHA would decrease due to the depressed stability and integrality of hairpin probes. To optimize the incubation temperature, the temperature ranges from 4 °C to 42 °C were evaluated by our experiments. Therefore, 25 °C was chosen as the optimal experiments (See in Fig. 4D).

< Fig. 4>

Dynamic range, sensitivity and selectivity

Under the optimal experimental conditions, the dynamic range and sensitivity of the proposed electrochemical sensor was confirmed (Tris–HCl, pH 7.4, containing 1 M NaCl). As shown in Fig. 5A, The SWV peak current increased with the increase of target miRNA concentration. The calibration plots showed a good linear relationship between the peak currents and the logarithm of target miRNA concentrations in the range from 100 fM to 2 nM (Fig. 5B). The linear regression equation was I (nA) = 117.0Log(C) + 137.7, with a correlation coefficient of 0.998 and the low detection limit reaches 30 fM from three times the standard deviation corresponding to the blank sample detection, thus make it suitable for miRNA real sample analysis. These results indicated our method shows sensitivity improvement compared traditional CHA (See in Fig. S5). The satisfactory detection limit and sensitivity could be mainly ascribed to the signal amplification of CHA, which were employed to make protector strand recycling. More comparisons of our work with previously reported similar methodologies from some different aspects are shown in Table S3.

< Fig. 5>

To test the selectivity of the developed method, we compared single-base mismatched target and miRNA target at the same concentration of 50 pM. As illustrated in Fig. 6A, the presence of the target miRNA resulted in a significantly enhanced response signal compared with that of the single-base mismatched target (with the calculated DF 48.2). This high DF is due to the thermodynamic preference of target miRNA rather than spurious miRNA for toehold exchange mediated SDA. The above results indicated that the biosensor displayed excellent selectivity for the determination of target miRNA.

The detection of rare content miRNA target with large amounts of interference miRNAs similar to target sequence still reminds a tremendous challenge. The reason is due to interference miRNAs similar in target sequence could consume significant number of reaction resources and generates non-specific signals. To solve this, SDR was used to silence the expression of interference miRNAs and enhance discrimination factor. As shown in Scheme 1B, only perfect matched target occur SDR to large extent and generates protector output for CHA. Whereas in the presence of spurious targets, SDR could not take place thus sink the protector output. To evaluate the assay ability to detect rare miRNA target with amounts miRNA interference similar in sequence, 50 pM miRNA target, the mixture of 20-fold (1 nM) spurious target and 50 pM miRNA target was analyzed. As shown in Fig. 6B, 50 pM pure miRNA target showed a remarkable 334 nA response current (RSD=2.3%, three repeat experiments) while current response of spurious miRNA target was similar to that of the blank. In the presence of 50 pM miRNA target and 1 nM spurious target mixture, 342 nA response current (RSD=2.6%, three repeat experiments) was recorded. The above results demonstrate that our proposed biosensor has the potential to detect rare miRNA of rarely 5%.

< Fig. 6>

Reproducibility and reusability of the strategy

In addition, five replicate measurements for miRNA target at 0.1 nM and 25 nM showed the relative standard deviations were 3.5% and 1.7%, respectively, suggesting this method had good reproducibility. To further estimate the reusability of the biosensor, repeated regenerations were carried out on the same electrode (details see in Text S3). The sensor could be regenerated 5 times

View Article Online
DOI: 10.1039/C7AN01224A

while the electrochemical response only decreased less than 10%, suggesting the same electrode could be reused 5 times at least. Therefore, the sensor can be reused by simply washing the analytes from the sensing surface, suggesting a reduced detection cost and a rapid detection process.

Real sample analysis

The application of the developed biosensing assay for real samples was examined by monitoring miRN-21 in the MCF-7 and HEK293 cells. The total RNA used for detection was diluted to 400 ng/μL with DEPC treated water and 10 μL of the RNA sample was used for the measurement. According to the simultaneously constructed calibration curve, the amount of miRNA-21 in the total RNA sample was estimated to be 2.4 fmol and 75.4 amol per 10 μL MCF-7 and HEK293 cells (See Text S4). To further evaluate its performance in real sample analysis and exclude the possible non-specific background signal, different amounts of miRNA-21 were spiked into MCF-7 total RNA for the assay, and the results showed the recovery of 99.1–105.0% (Table S4), suggesting that the method could sensitively detect miRNA in real samples.

Conclusions

In conclusion, we have developed a sensitive and selective electrochemical DNA biosensor by coupling strand displacement reaction and catalytic hairpin assembly. Moreover, the proposed biosensor could detect rare miRNAs with amounts of spurious analogues. This merit entrust our biosensor excellent performance in real sample analysis. In addition, the developed biosensor shows acceptable reproducibility, reusability and the designed biosensing methodology can conveniently be extended to detect other analytes by simple change the corresponding sequence. With these features above, the demonstrated method holds great potential for simple, stable, sensitive and low-cost detection of miRNA, as well as other biological analytes for early diagnosis of diseases and biomedical research.

Acknowledgments

This work was financially supported by Key project of Education Department of Sichuan (16ZA0181), Key project of Health and Family Planning Commission of Sichuan Province (16ZD036) and the Youth Foundation of Southwest Medical University (2017103).

Notes and references

1. A. Stark, J. Brennecke, N. Bushati, R. B. Russell and S. M. Cohen, Cell, 2005, 123, 1133-1146.
2. U. A. Ørom, F. C. Nielsen and A. H. Lund, Molecular cell, 2008, 30, 460-471.
3. N. Pinzón, B. Li, L. Martinez, A. Sergeeva, J. Presumey, F. Apparailly and H. Seitz, Genome Research, 2017, 27, 234-245.
4. J. R. Chevillet, T. D. Khokhlova, M. D. Giraldez, G. R. Schade, F. Starr, Y.-N. Wang, E. N. Gallichotte, K. Wang, J. H. Hwang and M. Tewari, Radiology, 2016, 283, 158-167.
5. Y. Wang, R. Medvid, C. Melton, R. Jaenisch and R. Blelloch, Nature genetics, 2007, 39, 380-385.
6. S. Nakamura, M. Horie, T. Daidoji, T. Honda, M. Yasugi, A. Kuno, T. Komori, D. Okuzaki, H. Narimatsu and T. Nakaya, Journal of virology, 2016, 90, 1788-1801.
7. M. Kayano, S. Higaki, J.-i. Satoh, K. Matsumoto, E. Matsubara, O. Takikawa and S. Niida, Biomarker Research, 2016, 4, 22.
8. K. W. Witwer, Clinical chemistry, 2015, 61, 56-63.
9. É. Várallyay, J. Burgyán and Z. Havelda, Nature protocols, 2008, 3, 190-196.
10. R. Petryszak, T. Burdett, B. Fiorelli, N. A. Fonseca, M. Gonzalez-Porta, E. Hastings, W. Huber, S. Jupp, M. Keays and N. Kryvych, Nucleic acids research, 2014, 42, D926-D932.
11. F. Marabita, P. de Candia, A. Torri, J. Tegnér, S. Abrignani and R. L. Rossi, Briefings in bioinformatics, 2016, 17, 204-212.
12. L. Cui, M. Lu, X.-y. Yang, B. Tang and C.-y. Zhang, *Analyst*, 2017, 142, 1562-1568.
13. T. Kilic, S. N. Topkaya, D. O. Ariksoysal, M. Ozsoz, P. Ballar, Y. Erac and O. Gozen, Biosensors and Bioelectronics, 2012, 38, 195-201.
14. K. M. Koo, L. G. Carrascosa, M. J. A. Shiddiky and M. Trau, Anal. Chem., 2016, 88, 2000–2005.
15. Y. Sun, K. J. Gregory, N. G. Chen and V. Golovlev, Analytical biochemistry, 2012, 429, 11-17.
16. Y.-Q. Yu, J.-P. Wang, M. Zhao, L.-R. Hong, Y.-Q. Chai, R. Yuan and Y. Zhuo, Biosensors and Bioelectronics, 2016, 77, 442-450.
17. Y. Xu, D. Li, W. Cheng, R. Hu, Y. Sang, Y. Yin, S. Ding and H. Ju, Analytica Chimica Acta, 2016, 936, 229-235.
18. S. Persano, M. L. Guevara, J. Wolfram, E. Blanco, H. Shen, M. Ferrari and P. P. Pompa, ACS omega, 2016, 1, 448-455.
19. H. Ravan, Analytica chimica acta, 2016, 910, 68-74.
20. J. Zhuang, W. Lai, G. Chen and D. Tang, Chemical communications, 2014, 50, 2935-2938.
21. H. Zhang, Q. Wang, X. Yang, K. Wang, Q. Li, Z. Li, L. Gao, W. Nie and Y. Zheng, Analyst, 2017, 142, 389-396
22. R. Deng, L. Tang, Q. Tian, Y. Wang, L. Lin and J. Li, Angewandte Chemie International Edition, 2014, 53, 2389-2393.
23. C. JamesáYang, Chemical Communications, 2014, 50, 1576-1578.
24. S. Cai, Z. Cao, C. Lau and J. Lu, Analyst, 2014, 139, 6022-6027.
25. F. Xuan and I.-M. Hsing, Journal of the American Chemical Society, 2014, 136, 9810-9813.
26. H. Dong, X. Meng, W. Dai, Y. Cao, H. Lu, S. Zhou and X. Zhang, Analytical chemistry, 2015, 87, 4334-4340.

View Article Online
DOI: 10.1039/C7AN01224A

27. N. Hao, X.-L. Li, H.-R. Zhang, J.-J. Xu and H.-Y. Chen, Chemical Communications, 2014, 50, 14828-14830.
28. A. A. Jamali, M. Pourhassan-Moghaddam, J. E. N. Dolatabadi and Y. Omidi, TrAC Trends in Analytical Chemistry, 2014, 55, 24-42.
29. Q. Wang, Q. Li, X. Yang, K. Wang, S. Du, H. Zhang and Y. Nie, Biosensors and Bioelectronics, 2016, 77, 1001-1007.
30. J. Yao, Z. Zhang, Y. Zhao, W. Jing and G. Zuo, RSC Advances, 2016, 6, 38869-38874.
31. D. Y. Zhang, S. X. Chen and P. Yin, Nature chemistry, 2012, 4, 208-214.
32. Z. Zhang, J. long Li, J. Yao, T. Wang, D. Yin, Z. Chen and G. Xie, Biosensors and Bioelectronics, 2016, 79, 488-494.
33. M. B. Baker, G. Bao and C. D. Searles, Nucleic acids research, 2011, 40, e13.
34. A. Idili, K. W. Plaxco, A. Vallée-Bélisle and F. Ricci, ACS nano, 2013, 7, 10863-10869.
35. L. A. Goff, M. Yang, J. Bowers, R. C. Getts, R. W. Padgett and R. P. Hart, RNA biology, 2005, 2, 93-100.
36. B. Li, A. D. Ellington and X. Chen, Nucleic acids research, 2011, 39, e110.

View Article Online
DOI: 10.1039/C7AN01224A

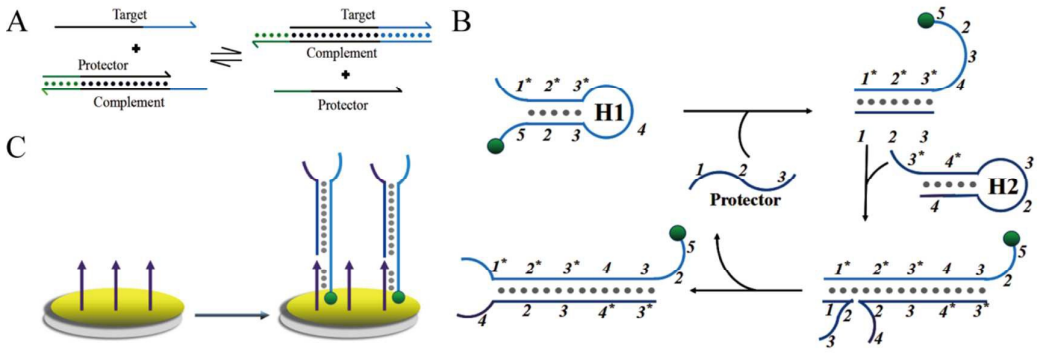

Scheme 1 Scheme illustration of the proposed (A) strand displacement reaction to generates protector output, (B) catalytic hairpin assembly to generates H1/H2 duplex output and (C) electrochemical signal generation procedure.

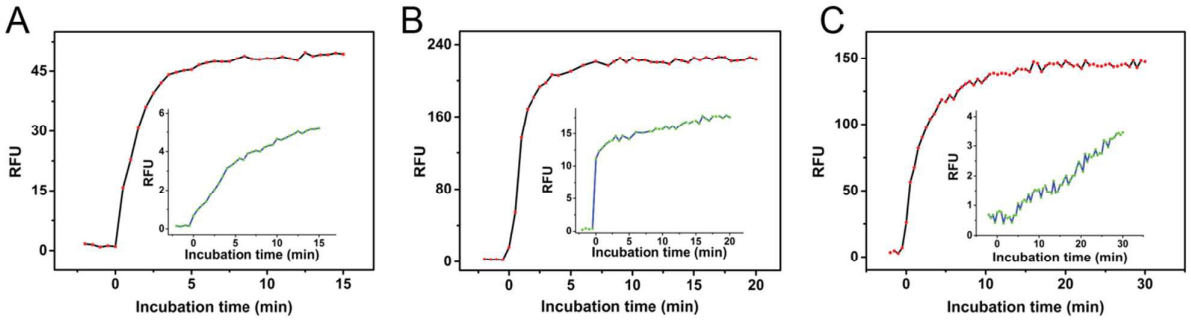

Fig. 1 Kinetic characterization of (A) SDR (B) CHA and (C) this proposed coupling strategy. The outside shows the kinetic of target miRNA-21 and the inset shows the spurious single base mismatch target.

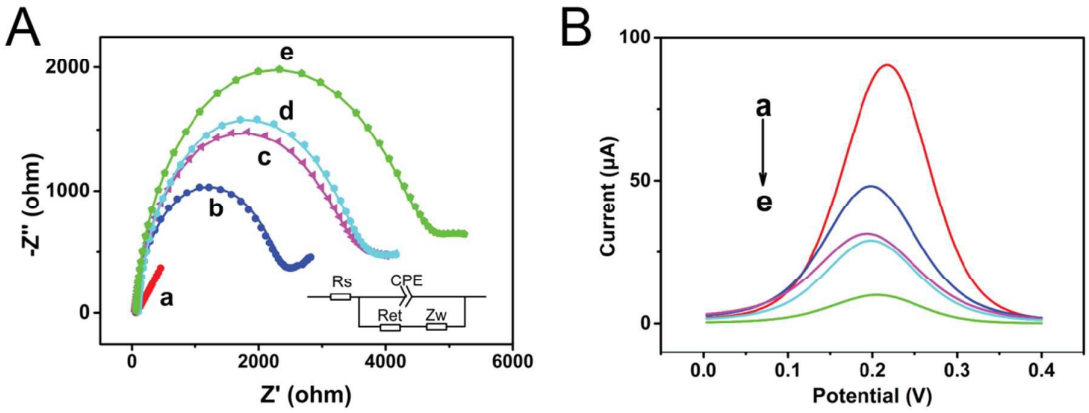

Fig. 2 EIS (A) and SWV (B) in 0.1 M KCl (pH 7.0) containing 5 mM $Fe(CN)_6^{3/4}$ at bare electrode (a), capture DNA modified electrode (b), MCH immobilized on the electrode surface (c), capture DNA modified electrode incubated without H1/H2 complexes (d) and capture DNA modified electrode hybridized with H1/H2 complexes with target miRNA-21 (e), respectively. The dotted line shows simulated data according to Randless circuit.

View Article Online
DOI: 10.1039/C7AN01224A

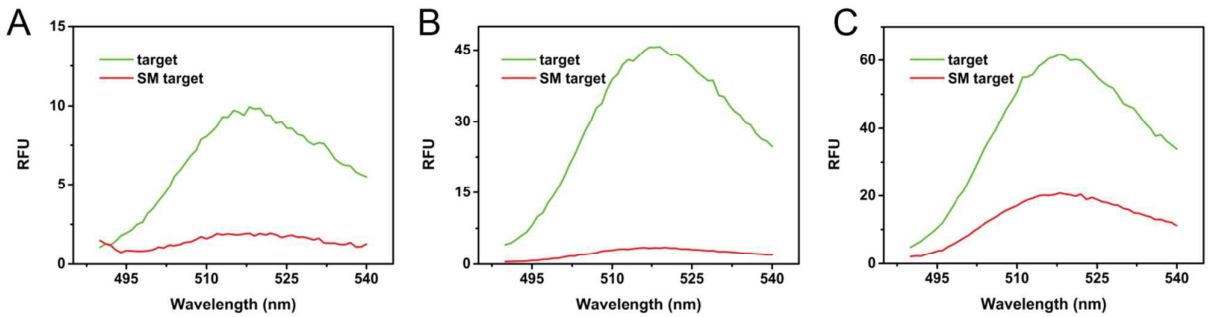

Fig. 3 Optimization the length of separation toeholds (A) 6 nt; (B) 4 nt and (C) 2 nt. The DF for 6 nt, 4 nt, 2 nt are 5.1, 12.8 and 3.0, respectively.

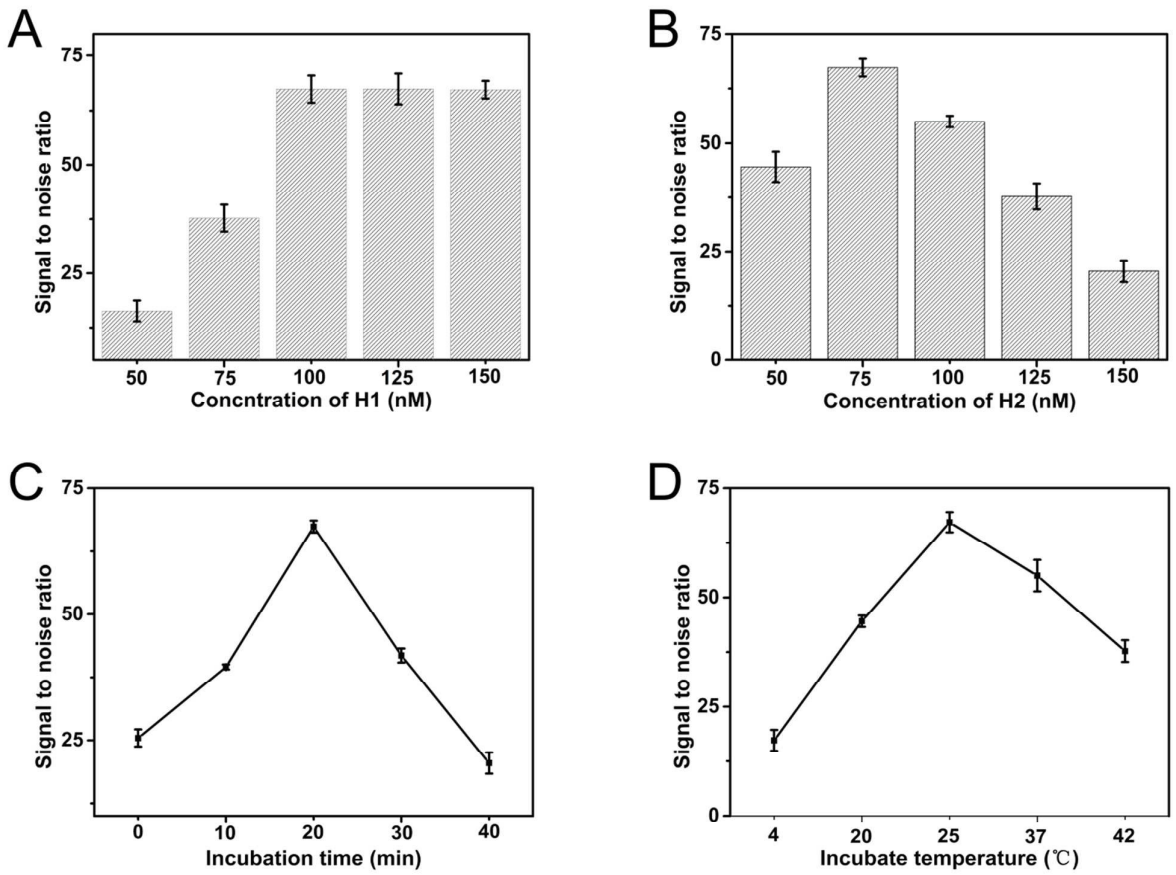

Fig. 4 Optimizations of experimental parameters (A) H1 concentration on signal to noise ratio, (B) H2 concentration on signal to noise ratio, (C) evaluation of the effect of incubation time on the signal to noise ratio, and (D) evaluation of the effect of incubation temperature on the signal to noise ratio. When one parameter changed, the others were under their optimal conditions. Error bars represent standard deviations of three measurements.

View Article Online
DOI: 10.1039/C7AN01224A

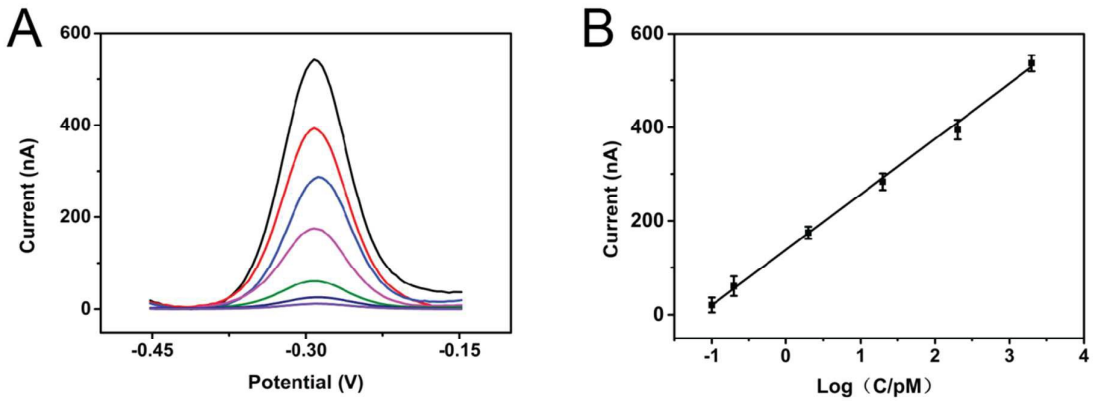

Fig. 5 (A) SWV responses and (B) the corresponding calibration curve to 0, 100 fM, 200 fM, 2 pM, 20 pM, 200 pM and 2 nM of target miRNA (from bottom to top) using strand displacement reaction coupled catalytic hairpin assembly. The reported SWV curves were background-subtracted with Origin 9 via extrapolation to the baseline. Error bars represent standard deviations of three measurements.

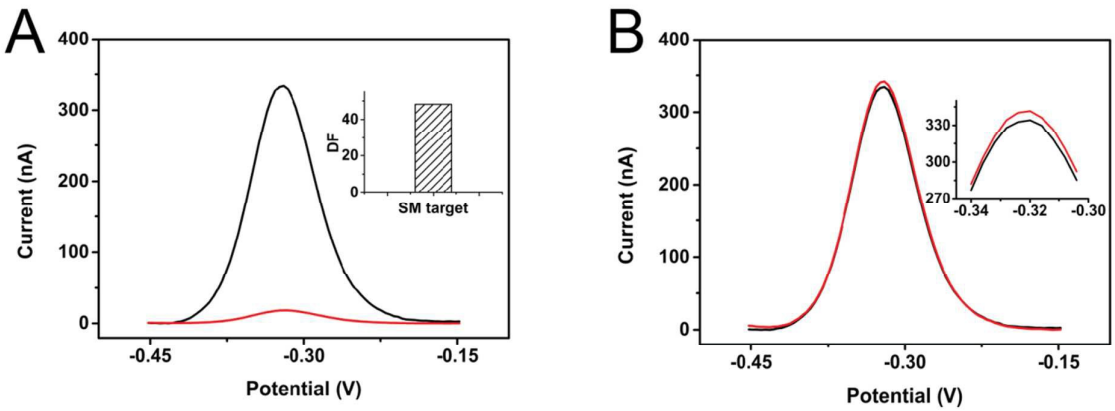

Fig. 6 (A) Specificity of the proposed electrochemical biosensor to perfectly matched target and SM target. (B) Rare mutation analysis of 50 pM miRNA target (black curve) and the mixture of 50 pM miRNA target and 1 nM spurious target (red curve). Inset shows the amplification signals.

View Article Online
DOI: 10.1039/C7AN01224A

An enzyme free electrochemical biosensor for sensitive detection of miRNA with high discrimination factor by coupling strand displacement reaction and catalytic hairpin assembly recycling

Juan Yao[a], Zhang Zhang[b], Zhenghua Deng[b], Youqiang Wang[a] and Yongcan Guo[a,*]

[a] Department of Laboratory Medicine, Affiliated Traditional Chinese Medicine Hospital of Southwest Medical University, Luzhou, China

[b] Department of Laboratory Medicine, Affiliated Hospital of Southwest Medical University, Luzhou, China

E-mail: swtcmlab@163.com and 396497795@qq.com

View Article Online
DOI: 10.1039/C7AN01224A

Text S1 Reproducibility analysis

The used biosensor surface (capture probe modified gold electrode and blocked with MCH) was renewed with the following processes. It was rinsed with 20 mM NaOH to remove the bound analytes on the gold film and washed with hybridization buffer for the next detection.

Capture probe surface density on gold electrode (the number of electroactive DNA moles per unit area of the active electrode surface) can be calculated from the redox charges of RuHex using as previously established chronocoulometry method (over a range of 0 to -0.5 V at a period 500 ms), first proposed by Tarlov and co-workers[1]. Before electrochemical experiments, the electrode was immersed in the solution for 5 min for adsorption equilibrium. Then chronocoulometry measurements were first performed in 10 mM Tris-HCl (pH 7.0) and compared with those in 10 mM Tris-HCl containing 50 μM RuHex. The surface density can be easily calculated from the equation as follows:

$$\Gamma_{DNA} = \left(\frac{QN_A}{nFA}\right)\left(\frac{z}{m}\right)$$

Where Γ_{DNA} is the probe surface density in molecules/cm^2, Q is the integrated charge of surface-confined RuHex obtained by calculating the chronocoulometric intercept at t=0, Q_{dl} is the integrated charge in the absence of RuHex (As shown in Figure S1). N_A is Avogadro's number, n is the number of electrons per molecule for reduction, F is the Faraday constant (C/equiv), A is the electrode area (cm^2), z is the charge of the redox molecule, and m is the number of nucleotides of capture probe.

View Article Online
DOI: 10.1039/C7AN01224A

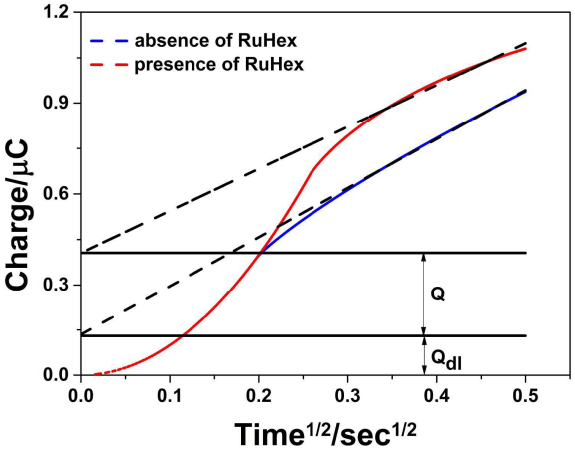

Figure S1. Chronocoulometry response curves for capture probe in the absence and presence of 50 μM RuHex in 10 mM Tris-HCl (pH 7.0)

The active surface area was measured using cyclic voltammetry, where the peak current is related to the surface area and the scan rate via the equation

$i_p=2.69\times10^5 n^{3/2} A D^{1/2} v^{1/2} C^o$

Where n is the number of electrons transferred in the reaction (for $Fe(CN)_6^{3/4}$, n=1), A is the active surface area of the electrode, D is the diffusion coefficient of the oxidant or reductant (6.9×10^{-6}cm^2/s for 1 mM $Fe(CN)_6^{3/4}$ in 0.1 M KCl solution), v is the scan rate, and C^o is the concentration of the oxidant or reductant (1mM $Fe(CN)_6^{3/4}$). Translated Eq. (1) to ip=kv$^{1/2}$. As shown in Figure S2, k is the slope of ip vs v$^{1/2}$and found to be 18.02×10^{-6}A s$^{1/2}$/V$^{1/2}$. The system exhibited a pair of distinct redox peak and suggesting facile surface-confined charge transfer kinetics. From above, active electrode surface can easily calculate to 0.028 cm^2 (RSD=1.4%, three repeat experiments).

View Article Online
DOI: 10.1039/C7AN01224A

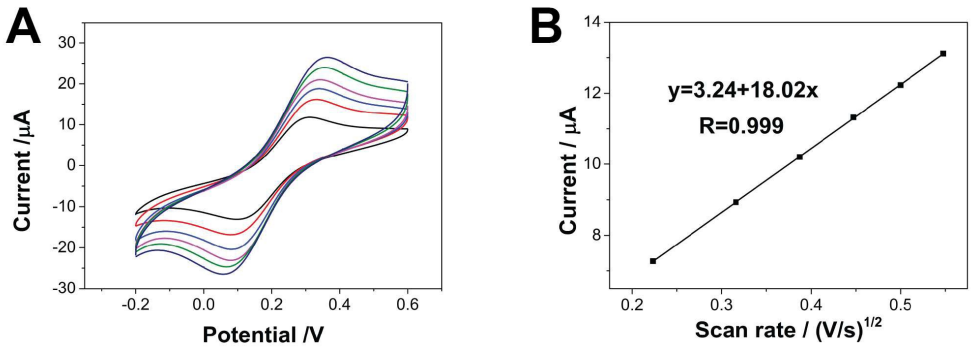

Figure S2. (A) Cyclic voltammetry and (B) Peak current vs. square root of different scan rates (50 mV, 100 mV, 150 mV, 200 mV, 250 mV and 300 mV) for bare electrode with 1 mM $Fe(CN)_6^{3/4}$ in 0.1 M KCl solution

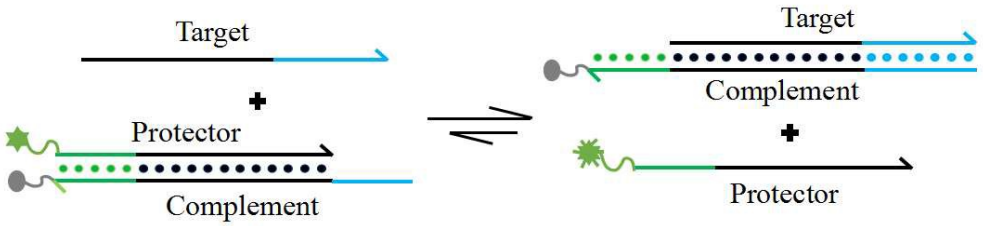

Figure S3 Scheme illustration of optimization experiments of separation toehold length (blue color: initial toehold; green color: separation toehold).

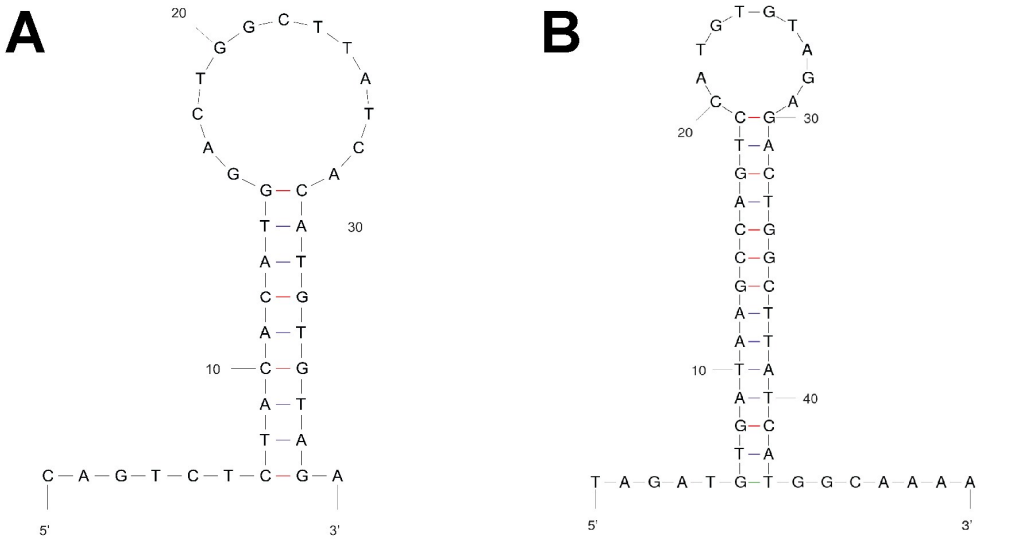

Figure S4 Thermodynamic prediction of the secondary structures of hairpin probes

View Article Online
DOI: 10.1039/C7AN01224A

and hybridization products using Mfold software.

Text S2 Analysis of traditional catalytic hairpin assembly

Under the optimal experimental conditions, the linear range and sensitivity of the traditional CHA electrochemical sensor was confirmed. As shown in Figure S5A, The SWV peak current increased with the increase of target miRNA concentration. The calibration plots showed a good linear relationship between the peak currents and the logarithm of target miRNA concentrations in the range from 1 pM to 10 nM (Figure S5B), the peak currents that responded to the target at higher or lower concentrations were beyond the linear response range. The resulting linear equation could be expressed as I (nA) = 157.8Log(C) + 76.5 (with a correlation coefficient of 0.997), with detection limit of 0.6 pM from three times the standard deviation corresponding to the blank sample detection (See in Figure S5).

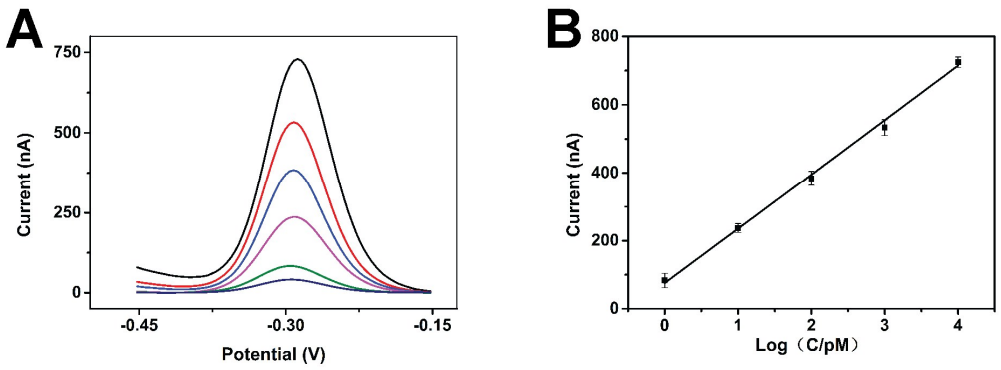

Figure S5 (A) SWV responses and (B) the corresponding calibration curve to 1 pM, 10 pM, 100 pM, 1 nM and 10 nM of target miRNA using traditional CHA amplification. The reported SWV curves were background-subtracted with Origin 9 via extrapolation to the baseline.

Text S3 Reusability of the sensing surface

The regeneration performance of the sensing interface is an important issue for practical implementation of biosensors. Therefore, the reusability of the DNA probe covalently immobilized to the sensing surface was evaluated. The sensor surface was

View Article Online
DOI: 10.1039/C7AN01224A

immersed with NaOH for 30 min and analyzed via chronocoulometry to calculate the probe density. The results showed that this sensor could be regenerated 5 times as the probe density remains 90% of initial.

Text S4

cDNA was utilized as a template to amplify target genes, along with SYBR Premix Ex Taq (Takara Bio Inc.). Each RNA sample was evaluated in triplicate. Forward primer: TGGCGTAGCTTATCAGACTGA and reverse primer: GTGCAGGGTCCGAGGT.

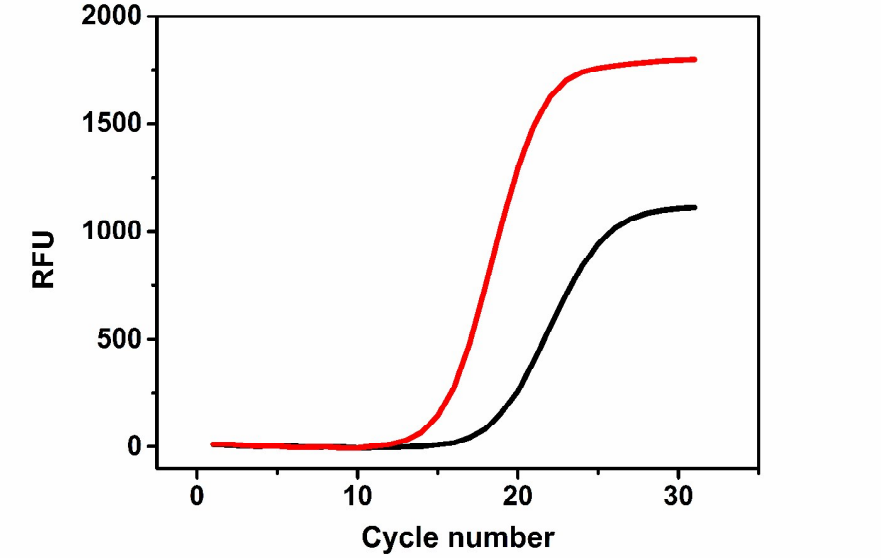

Figure S6 RT-qPCR validation of miR-21expression levels in the two MCF-7 and HEK293 cell lines.

Table S1 Sequences of the designed oligonucleotides

Oligonucleotides	Sequences(5' to 3')
Target	UAGCUUAUCAGACUGAUGUUGA
SM	UAGCUUAUCACACUGAUGUUGA
Complement 1	TCAACATCAGTCTGATAAGCTAGATGCA-Dabcyl

View Article Online
DOI: 10.1039/C7AN01224A

Protector1	FAM-TGCATCTAGCTTATCAGACTG
Complement 2	TCAACATCAGTCTGATAAGCTAGATG-Dabcyl
Protector 2	FAM-CATCTAGCTTATCAGACTG
Complement 3	TCAACATCAGTCTGATAAGCTAGA-Dabcyl
Protector 3	FAM-TCTAGCTTATCAGACTG
H1	TAGATGTGATAAGCCAGTCCATGTGTAGAGACTGGCTT ATCATGGCAAAA-MB
H2	CAGTCTCTACACATGGACTGGCTTATCACATGTGTAGA
Capture probe	5'SH-$(CH_2)_6$ TTTTGCCATGATAAGC

Note: SM, single-base-mismatched target

Table S2 Domain sequences of basic catalytic reaction

Domain	Sequence(5' to 3')	Length (nt)
1	CATCTA	6
2	GCTTATCA	8
3	GACTG	5
4	CATGTGTAGA	10
5	TGGCAAAA	8

Table S3 Comparison of different miRNA biosensors

Method	Form of signal amplification	Linear range	Detection limit	Reference
Fluorescent	DNA-templated copper nanoclusters	50 pM-10 nM	11 pM	[2]
Fluorescent	hybridization chain reaction	1.56 nM-400 nM	0.78 nM	[3]
Surface plasmon resonance	Gold nanorods-assisted signal amplification	00 fM-100 pM	45 fM	[4]
Colorimetry	hybridization chain reaction	1 pM-100 pM	31.8 fM and 100 fM	[5]
Electrochemistry	Pt nanoparticle	5.6 pM-560 nM	1.87 pM	[6]
Electrochemistry	strand displacement reaction and catalytic hairpin assembly	100 fM to 2 nM	30 fM	This work

View Article Online
DOI: 10.1039/C7AN01224A

Table S4 Recovery tests of miRNA -21

Sample	Spiking value (fmol)	Assayed value (fmol)	Recovery (%)
MCF-7 total RNA (400 ng)	-	2.4	-
Spike miRNA-21(1)	10	12.9	105.0
Spike miRNA-21(2)	100	101.5	99.1
Spike miRNA-21(3)	1000	996.1	99.4

References

[1] A.B. Steel, T.M. Herne, M.J. Tarlov, Electrochemical quantitation of DNA immobilized on gold, Analytical chemistry, 70 (1998) 4670-4677.

[2] Y.-S. Borghei, M. Hosseini, M.R. Ganjali, Fluorescence based turn-on strategy for determination of microRNA-155 using DNA-templated copper nanoclusters, Microchimica Acta, (2017) 1-7.

[3] X. Qiu, P. Wang, Z. Cao, Hybridization chain reaction modulated DNA-hosted silver nanoclusters for fluorescent identification of single nucleotide polymorphisms in the let-7 miRNA family, Biosensors and Bioelectronics, 60 (2014) 351-357.

[4] K. Hao, Y. He, H. Lu, S. Pu, Y. Zhang, H. Dong, X. Zhang, High-sensitive surface plasmon resonance microRNA biosensor based on streptavidin functionalized gold nanorods-assisted signal amplification, Analytica Chimica Acta, 954 (2017) 114-120.

[5] N. Ying, T. Sun, Z. Chen, G. Song, B. Qi, S. Bu, X. Sun, J. Wan, Z. Li, Colorimetric detection of microRNA based hybridization chain reaction for signal amplification and enzyme for visualization, Analytical Biochemistry, (2017).

[6] X. Wu, Y. Chai, R. Yuan, H. Su, J. Han, A novel label-free electrochemical microRNA biosensor using Pd nanoparticles as enhancer and linker, Analyst, 138 (2013) 1060-1066.